Journal of Atmospheric and Solar-Terrestrial Physics 70 (2008) 1366–1372

Contents lists available at ScienceDirect

Journal of Atmospheric and Solar-Terrestrial Physics

journal homepage: www.elsevier.com/locate/jastp

Diurnal and semidiurnal atmospheric tides observed by co-located GPS and VLBI measurements

Shuanggen Jin [a,*], Y. Wu [b], R. Heinkelmann [c], J. Park [a]

[a] Korea Astronomy and Space Science Institute, Daejeon 305-348, South Korea
[b] Key Laboratory of Geological Hazards in Three Gorges, Yichang, China
[c] Vienna University of Technology, Vienna 1040, Austria

ARTICLE INFO

Article history:
Received 6 February 2008
Received in revised form
13 March 2008
Accepted 2 April 2008
Available online 10 April 2008

Keywords:
Atmospheric tides
ZTD
VLBI
GPS

ABSTRACT

The tropospheric zenith total delay (ZTD) derived from very long baseline interferometry (VLBI) is an important parameter of the atmosphere, reflecting various atmosphere-related processes and variations. In this paper, ZTD time series of the IVS rapid combined tropospheric product (2002–2006) with a 1-h resolution are used for the first time to investigate the diurnal and semidiurnal oscillations. Significant diurnal and semidiurnal variations of ZTD are found at all VLBI stations. The amplitude of the diurnal cycle S_1 is 0.6–1.2 mm at most of the VLBI stations, and the amplitude of the semidiurnal cycle S_2 is 0.2–1.9 mm, which nearly accord with the surface pressure tides S_1/S_2 and co-located GPS estimated S_1/S_2. The results indicate that the S_1 and S_2 behaviors are mainly dominated by the hydrostatic component, namely pressure tides. In general, the semidiurnal S_2 amplitudes are slightly larger than the diurnal S_1. While S_1 shows no clear dependency on site altitude, S_2 has a regular distribution with VLBI site altitude. The results are in accordance with predictions of the classic tidal theory [Chapman, S., Lindzen, R.S., 1970. Atmospheric Tides, Gordon and Breach, New York].

1. Introduction

The tropospheric delay is one of the major error sources for space-geodetic observations at radio wavelengths, such as very long baseline interferometry (VLBI). Recently, VLBI has been widely used to determine the tropospheric zenith total delay (ZTD) (e.g., Davis et al., 1985; Gradinarsky et al., 2000; Krügel et al., 2007) through mapping functions (Niell, 1996). ZTDs from VLBI were compared with different techniques by various authors. For example, Behrend et al. (2000) analyzed about 2 weeks of data during December 1996 at Madrid (Spain) and found that the ZTD differences between VLBI and GPS were smaller than 1 cm. Niell et al. (2001) compared the results of a 2-week continuous VLBI campaign in August 1995 (CONT95) at Westford (USA) with GPS, water vapor radiometry (WVR) and radiosondes and concluded that the VLBI technique was the most accurate for the determination of ZTD. Snajdrova et al. (2005) analyzed 15 days of continuous VLBI data during the continuous VLBI campaign in 2002 (CONT02) and found that the ZTD from VLBI and GPS were in good agreement at the 3–10 mm level as well as with the Doppler Orbitography Radio positioning Integrated by Satellite. Meanwhile, VLBI- and GPS-determined ZTDs also show quite good agreements with those from the European Centre for Medium-Range Weather Forecasts (Heinkelmann et al., 2007) and WVR. Therefore, VLBI can provide highly precise and accurate estimates of ZTD for atmospheric and climatological applications.

In addition, the VLBI ZTD time series with 1-h time resolution can be used to study sub-diurnal variations. As the atmospheric density changes the refractive index of the zenith column of air under the influence of the atmospheric tides, which cause an oscillation in the ZTD at the tidal frequency, the oscillations at the solar day

* Corresponding author. Tel.: +82 42 865 3241; fax: +82 42 861 5610.
E-mail addresses: sgjin@kasi.re.kr, sg.jin@yahoo.com (S. Jin).

1364-6826/$ - see front matter © 2008 Elsevier Ltd. All rights reserved.
doi:10.1016/j.jastp.2008.04.005

(diurnal) and half solar day (semidiurnal) periods in ZTD possibly reflect the diurnal and semidiurnal tides induced on the atmosphere by thermal and gravitational excitation from the Sun (Humphreys et al., 2005). If this explanation is supported by VLBI ZTD, it raises new applications to study atmospheric tidal phenomena with the VLBI technique. The atmospheric tides play an important role in the general circulation and coupling between the lower and the middle and upper atmosphere (Vial, 1989; Forbes, 1995; Hagan, 2000). Knowledge about the tides is also important for the analysis of satellite data sampled at different local solar times, data assimilation (Swinbank et al., 1999) and temperature trend estimation (Keckhut et al., 2001). Current techniques used for studying atmospheric tides include rocket- or balloon-born instruments, radar, geomagnetic field measurements, and, predominantly, surface pressure measurements. A great majority of atmospheric tidal analyses have been done using surface data. This is doubtless due to the relative ease and low cost of making surface measurements compared to balloon, rocket, or radar measurements. But the atmospheric tidal effects are dominated by meteorological noise (daily variations in weather) near the surface of the Earth. Although many authors have presented comprehensive empirical investigations of the solar diurnal tide (S_1) and the solar semidiurnal tide (S_2) over the past 30 years, there are still uncertainties in the characterization of the tidal variability due to the lack of observations.

In this paper, the ZTD time series from VLBI measurements are used for the first time to study diurnal and semidiurnal variations. By comparing with diurnal cycles in surface pressure, it shows the capability of VLBI detecting diurnal and semidiurnal atmospheric tide variations. In the following section the tidal oscillations and theory about the ZTD are briefly described. The diurnal and semidiurnal ZTD variations determined by VLBI are analyzed and compared with surface pressure and GPS at co-located sites in Section 3. Discussion and conclusions are given in Sections 4 and 5.

2. VLBI ZTD and atmospheric tides effect

2.1. IVS rapid combined ZTD time series

Eight analysis centers (ACs) of the International VLBI Service for Geodesy and Astrometry (IVS) process IVS-R1 and -R4 type of sessions VLBI observation data using three independent software packages, OCCAM, CALC/SOLVE, and SteelBreeze. The products (e.g. ZTD) are transferred to the Institute of Geodesy and Geophysics (IGG, Vienna University of Technology, Austria), for comparison and combination. The IVS ACs are the Bundesamt für Kartographie und Geodäsie (BKG, Germany), Centro di Geodesia Spaziale (CGS, Italy), CNR (Istituto di Radioastronomia, Italy), NASA Goddard Space Flight Center (GSFC, USA), Institute of Applied Astronomy (IAA, Russia), Institute of Geodesy and Geophysics (IGG, Vienna University of Technology, Austria), Main Astronomical Observatory (MAO, National Academy of Sciences of Ukraine, Ukraine), and Onsala Space Observatory (OSO, Sweden). GSFC

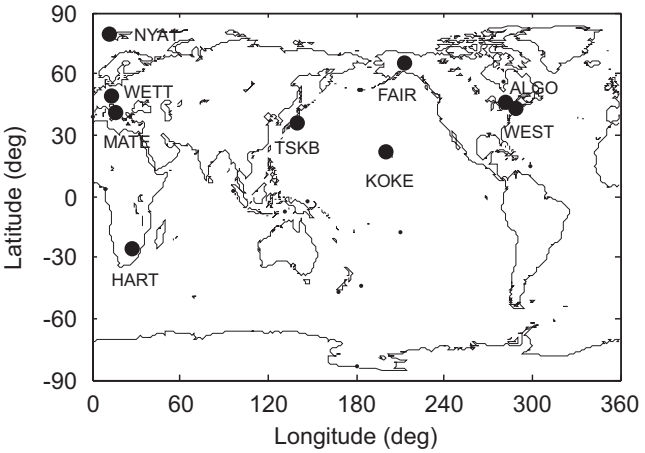

Fig. 1. The distribution of co-located VLBI and GPS sites.

maintains CALC/SOLVE and MAO, National Academy of Sciences of Ukraine maintains the SteelBreeze, while OCCAM is used in various versions developed by different ACs (Titov et al., 2004), e.g., at IAA, Russia. As individual ACs use different analysis software with different parameters and models, such as the thresholds of outlier detection, or elevation cutoff angles, it inevitably results in small but systematical differences for ZTD estimates between the solutions of the ACs. The combined ZTD product averages out those systematic differences and provides a robust and reliable basis for tropospheric parameters. For each integer hour for which at least two ACs have ZTDs, a combined ZTD is computed using a stepwise procedure. Outliers are eliminated from each time series exceeding a k-σ-threshold and relative weight factors are determined for each station and AC. These are used to compute the combined ZTDs as a weighted sum of the individual AC ZTDs. The detailed procedures are refereed to Schuh and Boehm (2003). Here nine co-located VLBI and GPS sites (Fig. 1) are selected with at least 4 years of observations from 2002 to 2006. For example, Fig. 2 (upper two panels) shows the VLBI ZTD and surface pressure time series at Gilmore Creek (FAIR), USA, and the two bottom panels are the short-period time series, which reflects a consistent variation pattern between ZTD and surface pressure, possibly indicating a connection between VLBI ZTD and atmospheric tides.

2.2. Atmospheric tides effect on ZTD

Due to the solar gravitational potential, thermal excitation by solar radiation and upward eddy conduction of heat from the ground, it has generated internal gravity waves in the atmosphere at periods of a solar day (primarily at the diurnal and semidiurnal periods). These waves cause regular oscillations in atmospheric temperature, wind velocity, and pressure, which are often referred to as atmospheric tides (Chapman and Lindzen, 1970; Whiteman and Bian, 1996). The solar diurnal and semidiurnal atmospheric tides are written as S_1 and S_2, respectively. In recent three decades, several studies of global atmospheric pressure variations have been carried out using empirical models or observation data, leading to

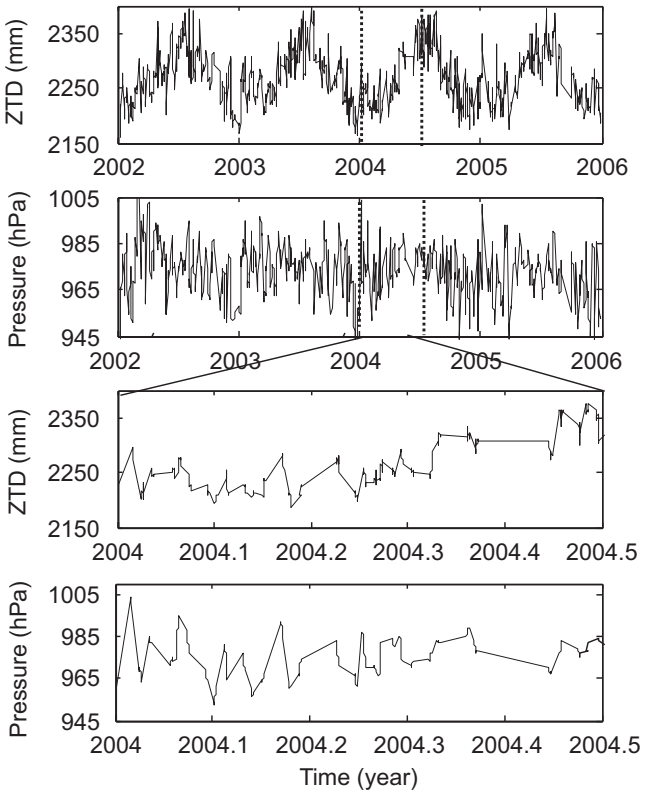

Fig. 2. Tropospheric total zenith delay (ZTD) and surface pressure time series at Gilmore Creek (FAIR), USA. From top to bottom: ZTD and pressure time series from 2002 to 2006, and corresponding parameters within swath box in upper two panels, respectively.

the development of the classic tidal theory (Chapman and Lindzen, 1970). For example, Groves and Wilson (1982) reported that solar heating can explain much more amplitudes in the S_1 and S_2. Dai and Wang (1999) found that the heating effects on S_1 are from the ground using surface pressure fields. Although lots of progresses on the tides have been made in the past one century, there are still uncertainties in the characterization of the tidal variability due to the lack of observations as well as verification by other techniques.

The VLBI-derived ZTD is the integrated refractivity along a vertical path through the neutral atmosphere:

$$ZTD = c\tau = 10^{-6}\int_0^{\infty} N(s)\mathrm{d}s \tag{1}$$

where c is the speed of light in a vacuum,τ is the delay measured in units of time and N is the neutral atmospheric refractivity. N is empirically related to standard meteorological variables as (Davis et al., 1985)

$$N = k_1\rho + k_2\frac{P_w}{Z_w T} + k_3\frac{P_w}{Z_w T^2} \tag{2}$$

where $k_i(i = 1,2,3)$ is the constant, ρ is the total mass density of the atmosphere, P_w is the partial pressure of water vapor, Z_w is a compressibility factor near unity accounting for the small departures of moist air from an ideal gas, and T is the temperature in degrees Kelvin. The integral of the first term of Eq. (2) is the hydrostatic component (N_h) of refractivity and the integral of the remaining two terms is the wet component (N_w) of refractivity. Thus, ZTD is the sum of the hydrostatic or 'dry' delay (ZHD) and non-hydrostatic or 'wet' delay (ZWD), due to the effects of dry gases and water vapor, respectively. The dry component ZHD accounts for about 90% of ZTD. It derives from the relationship with hydrostatic equilibrium approximation for the atmosphere. Under the assumption of hydrostatic equilibrium, the change in pressure with height is related to total density at the height h above the mean sea level by

$$\mathrm{d}p = -\rho(h)g(h)\mathrm{d}h \tag{3}$$

where $\rho(h)$ and $g(h)$ are the density and gravity at height h, respectively. It can be further deduced as

$$ZHD = kp_0 \tag{4}$$

where k is constant (2.28 mm/hPa) and p_0 is the pressure at height h_0 (Davis et al. 1985), where the scale factor varies less than 1% even under severe weather conditions. It shows that the ZHD is proportional to the atmospheric pressure at the site. As the hydrostatic component ZHD accounts for approximately 90% of ZTD, ZTD$\cong$ZHD/90% = 2.53 p_0. Given that surface pressure tide varies with 1 hPa, it nearly corresponds to 2.53 mm variation in the amplitude of ZTD.

3. Diurnal and semidiurnal atmospheric tides

As the VLBI-derived ZTD time series with 1-h interval are discrete, here the mean diurnal ZTD medians are obtained from the ZTD time series for the 2002–2006 periods at each co-located VLBI and GPS site in the globe. Fig. 3 shows the mean diurnal ZTD and surface pressure medians (solid line) at the VLBI site of Gilmore Creek (FAIR), USA. The dashed lines are the fitting ZTD and surface pressure time series with the following harmonic function. It has shown clear sub-diurnal ZTD variations, agreeing well with mean sub-diurnal pressure cycles, reflecting the regular sub-diurnal tides induced on the atmosphere by solar thermal and gravitational excitations.

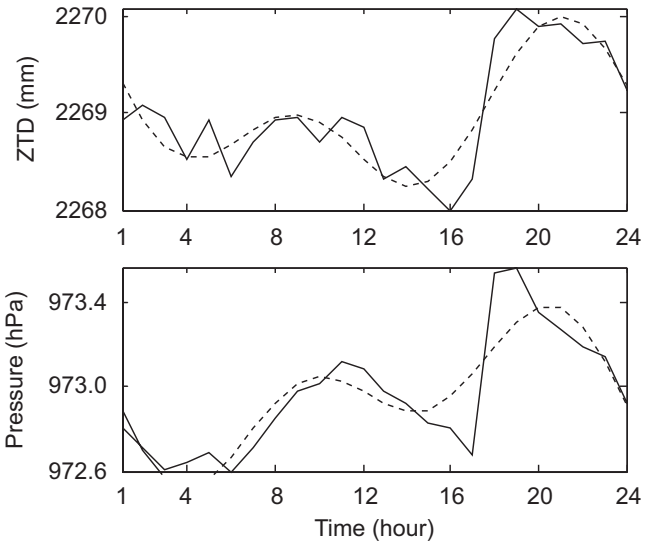

Fig. 3. Mean diurnal ZTD and surface pressure time series (solid line) at the VLBI site of Gilmore Creek (FAIR), USA. The dashed lines are the fitting ZTD (top) and surface pressure time series (bottom), respectively.

The VLBI ZTD time series are analyzed by a harmonic function with a linear trend, diurnal component (S_1), and semidiurnal component (S_2) as following

$$ZTD_t = a + bt + \sum_{k=1}^{2}[S_k \sin(2\pi(t - t_0)/p_k + \varphi_k)] + \varepsilon_t \quad (5)$$

where t is the time, a and b are the constant and linear terms, S_k and φ_k are the amplitude and phase at period $p_k(= 1, 1/2$ days), respectively, and ε_t is the residual. Using the time series of VLBI ZTD, we apply the method of least squares to determine the unknown parameters, e.g. magnitudes of VLBI ZTD variations with uncertainties in diurnal and semidiurnal time scales in Table 1. The mean uncertainty of diurnal and semidiurnal ZTD variations is about 0.02 mm.

In order to explain the diurnal and semidiurnal cycles of the VLBI-ZTD, we further compare the VLBI-ZTD diurnal cycle amplitude and phase with the surface pressure data. For example, the mean ZTD at the VLBI site of FAIR is approximately 2269 mm and the mean pressure is 973 hPa (Fig. 3), which yields a proportionality constant of 2.33 mm/hPa. The mean subdiurnal atmospheric tide amplitudes S_1 and S_2 at FAIR are 0.21 ± 0.01 and 0.22 ± 0.01 hPa (see Table 1), which correspondingly produce approximate 0.49 and 0.51 mm in diurnal and semidiurnal ZTD variations due to the S_1 and S_2 tides. This compares well with the 0.57 ± 0.02 and 0.53 ± 0.02 mm empirical amplitudes in diurnal and semidiurnal ZTD variations from the VLBI data at FAIR. Furthermore, the phases of S_1 and S_2 variation are nearly consistent between VLBI-derived ZTD and surface pressure data. It has been indicated that the VLBI ZTD data can detect the diurnal and semidiurnal atmospheric tide variations. In the following, the diurnal and semidiurnal tidal oscillations in ZTD are analyzed and their distributions are presented.

Fig. 4 shows the mean amplitudes of the diurnal cycle derived from the VLBI ZTD data (i.e., S_1 in Eq. (5)). It can be seen that most amplitudes of S_1 are about 0.6–1.2 mm. The other especially stronger diurnal amplitudes are found at the two middle-low latitude sites, MATE (Matera, Italy, near Mediterranean Sea) and KOKE (Kokee, Pacific) with about 5.1–7.1 mm. Fig. 5 shows the mean amplitude of the semidiurnal cycles derived from the VLBI ZTD data (i.e., S_2 in Eq. (5)). The magnitudes of S_2 are almost close to the S_1, with about 0.2–1.9 mm, excluding the sites MATE and KOKE with the especially stronger S_1 amplitude. Some semidiurnal S_2 amplitudes are a little larger than the diurnal S_1, such as WEST (Westford, USA), TSKB (Tsukuba, Japan), and HART (Hartebeesthoek, South Africa). However, the distributions of S_1 and S_2 with the latitude have a nearly consistency, namely that the amplitude reduces with the increasing latitude in the Southern and Northern Hemispheres (Fig. 6 and 7). Fig. 8 and 9 show the distribution of S_1 and S_2 with the altitude. S_2 is normally

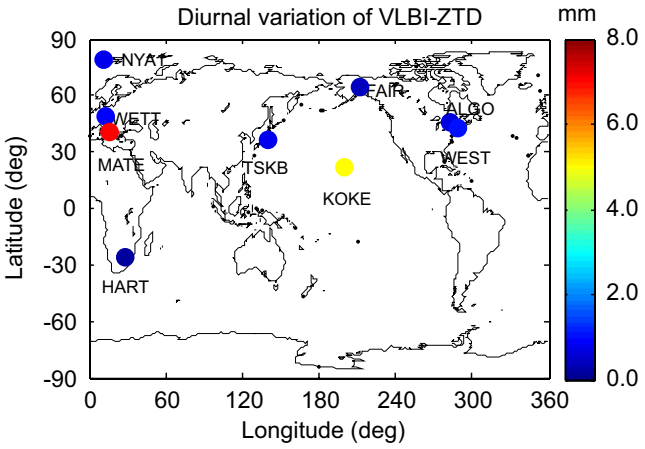

Fig. 4. Diurnal variation amplitude of ZTD at VLBI sites.

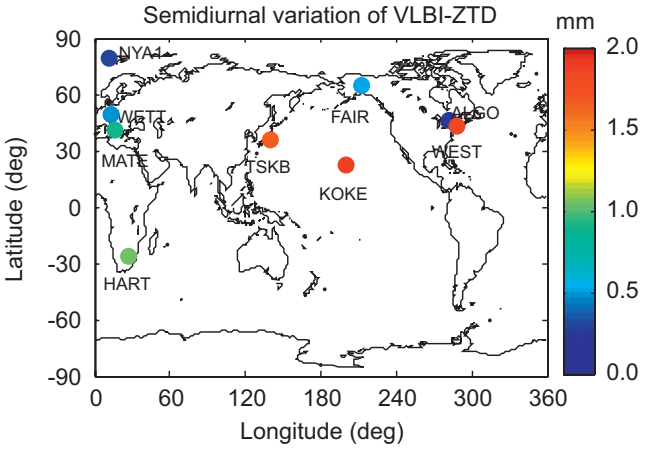

Fig. 5. Semidiurnal variation amplitude of ZTD at VLBI sites.

Table 1
Diurnal and semidiurnal variations determined by VLBI-/GPS-ZTD and surface pressure

Site	Lat	Lon	VLBI-ZTD (mm)		GPS-ZTD (mm)		Pressure (hPa)	
			S_1	S_2	S_1	S_2	S_1	S_2
ALGO	45.96	281.93	0.82 ± 0.02	0.21 ± 0.01	0.27 ± 0.01	0.27 ± 0.01	0.31 ± 0.01	0.30 ± 0.01
FAIR	64.98	212.50	0.57 ± 0.02	0.53 ± 0.02	0.76 ± 0.02	0.29 ± 0.01	0.21 ± 0.01	0.22 ± 0.01
HART	−25.89	27.69	0.22 ± 0.01	1.07 ± 0.03	0.09 ± 0.01	1.11 ± 0.03	0.96 ± 0.01	0.81 ± 0.02
KOKE	22.13	200.34	5.07 ± 0.02	1.91 ± 0.04	4.90 ± 0.27	2.42 ± 0.08	0.13 ± 0.01	0.84 ± 0.02
MATE	40.65	16.70	7.07 ± 0.21	0.93 ± 0.02	4.51 ± 0.23	0.60 ± 0.02	0.23 ± 0.01	0.35 ± 0.01
NYA1	78.93	11.87	0.87 ± 0.02	0.32 ± 0.01	0.38 ± 0.01	0.09 ± 0.01	0.27 ± 0.01	0.13 ± 0.01
TSKB	36.11	140.09	0.84 ± 0.02	1.67 ± 0.14	2.79 ± 0.08	1.14 ± 0.04	0.83 ± 0.01	0.97 ± 0.03
WEST	42.61	288.51	1.17 ± 0.04	1.89 ± 0.05	1.23 ± 0.03	0.50 ± 0.02	0.60 ± 0.01	0.50 ± 0.01
WETT	49.14	12.88	1.01 ± 0.03	0.52 ± 0.02	1.14 ± 0.03	0.57 ± 0.02	0.12 ± 0.01	0.36 ± 0.01

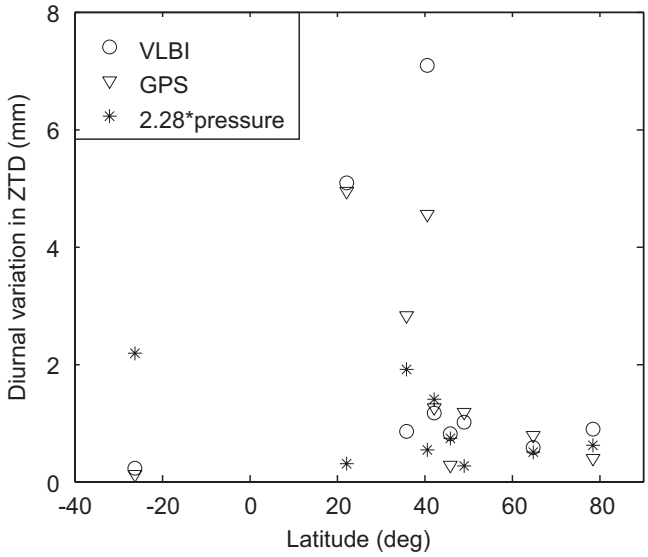

Fig. 6. Distribution of diurnal ZTD amplitude with the latitude.

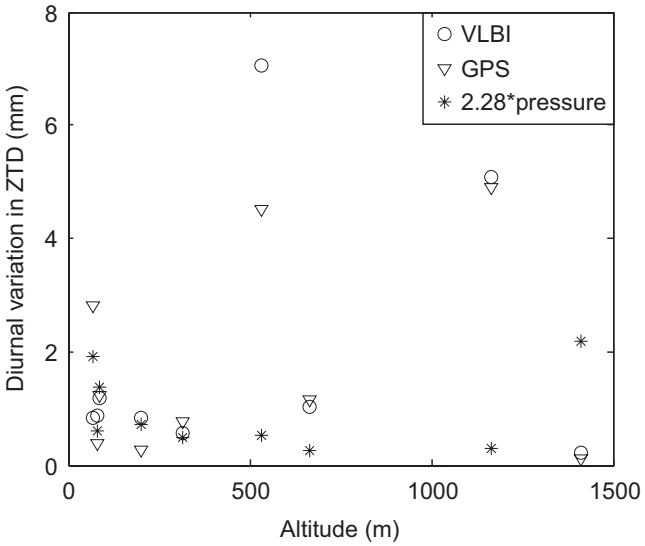

Fig. 8. Distribution of diurnal ZTD amplitude with the altitude (above the global mean sea level).

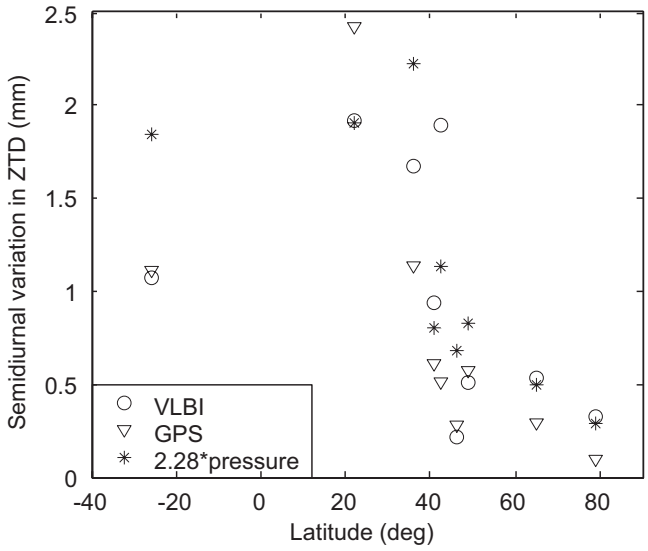

Fig. 7. Distribution of semidiurnal ZTD amplitude with the latitude.

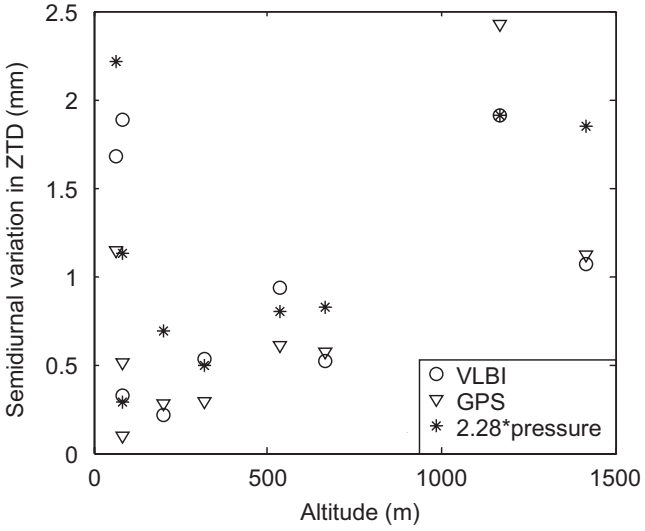

Fig. 9. Distribution of semidiurnal ZTD amplitude with the altitude.

increasing with the increasing altitude at VLBI site, while S_1 has irregular distribution with the altitude. The VLBI ZTD-derived S_1 and S_2 are almost the same as the surface pressure results (seeing Fig. 6–9), excluding two special VLBI sites MATE and KOKE with the particularly stronger S_1 amplitude, which will be discussed in the next section. The classic tidal theory predicts that the semidiurnal tide S_2 is thought to predominate over much of the globe, and is regularly distributed in its amplitude, while the diurnal tide S_1 is very irregularly distributed (Chapman and Lindzen 1970). This is also supported by our study with VLBI ZTD-derived tides and surface pressure measurements.

4. Discussion

Though the diurnal and semidiurnal atmospheric tides are well observed by the VLBI ZTD, it needs to be further checked by another independent technique. The GPS ZTD time series with temporal resolution of 2 h from 2002 to 2006 at the co-located VLBI sites are obtained by the GAMIT software (King and Bock, 1999), where the ZTD and other parameters are solved using a constrained batch least squares inversion procedure and the newly recommended strategies (Byun et al., 2005; Jin et al., 2007). Using the same harmonic analysis methods of Eq. (5), the diurnal and semidiurnal variations of the GPS ZTD are obtained (Table 1). The GPS ZTD-derived S_1 and S_2 variations are almost the same with the VLBI ZTD results (Fig. 6–9). The mean diurnal medians of pressure and ZTD are converted into diurnal anomalies by removing the daily mean for each day. For example, Fig. 10 shows the diurnal residual series of the ZTD and the pressure at co-located VLBI and GPS sites HART and WETT (Wettzell, Germany). It can be seen that the significantly consistent diurnal signals exist in VLBI and GPS ZTD as well as the

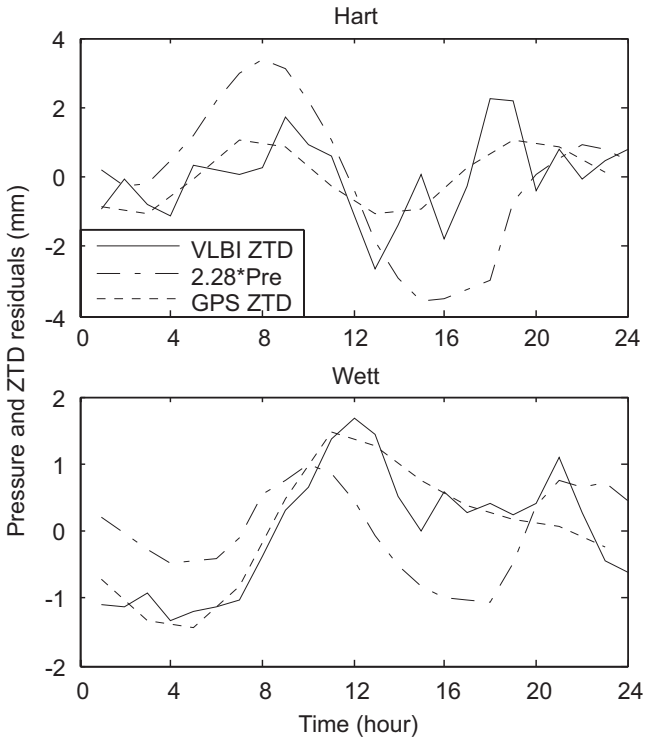

Fig. 10. Atmospheric parameters residuals at co-located VLBI and GPS sites HART and WETT.

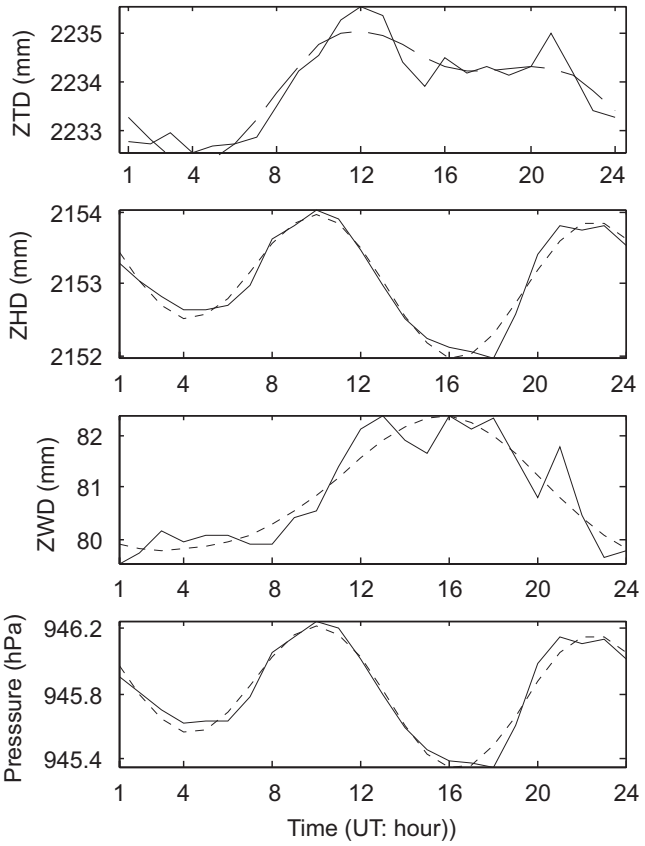

Fig. 11. The mean diurnal atmospheric parameters time series (solid line) at the VLBI site of Wettzell (WETT), Germany. From top to bottom: ZTD, ZHD, ZWD, and pressure time series. The dashed line is the fitting variations of the diurnal+semidiurnal atmospheric parameters time series.

surface pressure. Meanwhile, the S_1 and S_2 together can represent the diurnal variations very well. Only the anomalous S_1 amplitudes at the two VLBI sites (MATE near Mediterranean Sea and KOKE in Pacific) are largely different with the diurnal atmospheric tide. However, the S_1 amplitudes are almost the same confirmed by the co-located GPS sites (MATE and KOKE), which might explain that the marine-influenced atmosphere produces a seasonally varying diurnal oscillation in S_1.

Other processes may induce diurnal variations in ZTD, e.g. water vapor and atmospheric large-scale vertical motion, etc. Here we further investigate the wet component impact on the tides S_1 and S_2 variations, which probably explains some of the irregularity of the sub-diurnal VLBI ZTD variations relative to surface pressure. Fig. 11 is the mean diurnal atmospheric parameters time series (solid line) at the VLBI site WETT. From top to bottom it is the ZTD, ZHD, ZWD, and pressure time series, respectively. The dashed line is the fitting variations of the diurnal+semidiurnal atmospheric parameters time series. It can be seen that the ZTD almost reflects completely the diurnal+semidiurnal variations of the surface pressure or hydrostatic component (ZHD), particularly the obvious semidiurnal variation S_2, while the wet component (ZWD) does not have the same pattern. Dai et al. (2002) detected a ~0.1-mm semidiurnal variation in GPS-derived precipitable water vapor (PWV) estimates over North America, amounting to a ~0.7-mm semidiurnal variation in Zenith Wet Delay (ZWD), but conclusively demonstrated that the semidiurnal variation is much smaller than the root mean square errors for GPS-derived PWV and was not visible in independent radiosonde and WVR measurements. Such results further confirm the periodic variations in VLBI ZTD data, which are accepted as manifestations of atmospheric tides.

In addition, the VLBI-derived diurnal atmospheric tides may be affected by mapping function, solid earth tides, etc. Atmospheric pressure loading due to variations in surface pressure leads to slight deformation of VLBI sites (Petrov and Boy, 2004) and may be the possible error source for S_1 and S_2. However, a recent simulation study of the effects of atmospheric pressure loading on ZTD was conducted and found that atmospheric pressure loading effects on ZTD estimates amounted to less than 11% of the amplitude of the sub-diurnal oscillations in ZTD (Humphreys et al., 2005). Other error source is the mapping function. Humphreys et al. (2005) estimated that the impact of the mapping functions by Niell (1996) is less than 11% on the amplitude of the subdiurnal oscillations in ZTD, assuming an average distribution of elevation angles and an elevation cutoff of 7°. Finally, the limited VLBI stations and non-continuous VLBI observations may affect the S_1 /S_2 estimations, and it needs to be further investigated in the future. In general, the strong correlation with S_1 and S_2 mainly reflects that the diurnal and semidiurnal variations in VLBI ZTD data are due primarily to the actual diurnal and semidiurnal variations in atmospheric tides.

5. Conclusion

The diurnal and semidiurnal variations of tropospheric ZTD time series with 1-h interval from VLBI data of 2002–2006 are analyzed at nine co-located VLBI and GPS sites in the globe. The significant diurnal and semidiurnal variations of ZTD are found at all VLBI stations and moreover are in almost agreement with those derived from the co-located GPS sites and surface pressure data. The results indicate that the S_1 and S_2 behaviors mainly dominated by its hydrostatic component, namely pressure tides. The diurnal (24 h) cycle, S_1, with an amplitude of about 0.6–1.2 mm and the semidiurnal (12 h) cycle, S_2, with an amplitude of about 0.2–1.9 mm, explains well the sub-daily ZTD variation. The semidiurnal S_2 amplitudes at some VLBI sites are a little larger than the diurnal S_1. The S_2 are normally increasing with the increase of VLBI site altitude, while the S_1 has an irregular distribution with the altitude. These results are also supported by the classic tidal theory prediction that the semidiurnal tide S_2 is thought to predominate over much of the globe, and is regularly distributed in its amplitude, while the diurnal tide S_1 is very irregularly distributed (Chapman and Lindzen, 1970). Therefore, the precisely VLBI-observed ZTD possibly offers a tool to study atmospheric tides.

Acknowledgements

Authors thank referees for their valuable suggestions to greatly improve the paper. We also thank IVS for providing highly precise VLBI products. This work was supported by a grant (07KLSGC02) from Cutting-edge Urban Development-Korean Land Spatialization Research Project funded by Ministry of Land, Transport and Maritime Affairs.

References

Behrend, D., Cucurull, L., Vila, J., Haas, R., 2000. An inter-comparison study to estimate zenith wet delays using VLBI, GPS, and NWP models. Earth Planets Space 52, 691–694.

Byun, S.H., Bar-Sever, Y., Gendt, G., 2005. The new tropospheric product of the International GNSS service. Paper presented at 2005 ION GNSS Conference, Institute of Navigation, Long Beach, California.

Chapman, S., Lindzen, R.S., 1970. Atmospheric Tides. Gordon and Breach, New York.

Dai, A., Wang, J., 1999. Diurnal and semidiurnal tides in global surface pressure data. Journal of the Atmospheric Sciences 56, 3874–3891.

Dai, A., Wang, J., Ware, R.H., Van Hove, I., 2002. Diurnal variation in water vapor over North America and its implications for sampling errors in radiosonde humidity. Journal of Geophysical Research 107(D10), 4090, doi:10.1029/2001JD000642.

Davis, J., Herring, T.A., Shapiro, I.I., Rogers, A.E.E., Elgered, G., 1985. Geodesy by radio interferometry: effects of atmospheric modeling errors on the estimates of baseline lengths. Radio Science 20, 1593–1607.

Forbes, J.M., 1995. Tidal and planetary waves. Geophysics Monographs 87, 67–87.

Gradinarsky, L.P., Haas, R., Elgered, G., Johansson, J.M., 2000. Wet path delay and delay gradients inferred from microwave radiometer, GPS and VLBI observations. Earth Planets Space 52, 695–698.

Groves, G.V., Wilson, A., 1982. Diurnal, semi-diurnal and terdiurnal Hough components of surface pressure. Journal of Atmospheric and Terrestrial Physcs 44, 599–611.

Hagan, M.E., 2000. Modeling atmospheric tidal propagation across the stratopause. Geophysics Monographs 123, 177–190.

Heinkelmann, R., Boehm, J., Schuh, H., Bolotin, S., Engelhardt, G., MacMillan, D.S., Negusini, M., Skurikhina, E., Tesmer, V., Titov, O., 2007. Combination of long time-series of troposphere zenith delays observed by VLBI. Journal of Geodesy 81, 483–501.

Humphreys, T.E., Kelley, M.C., Huber, N., Kintner Jr, P.M., 2005. The semidiurnal variation in GPS-derived zenith neutral delay. Geophysical Research Letters 32, L24801.

Jin, S.G., Park, J.U., Cho, J.H., Park, P.H., 2007. Seasonal variability of GPS-derived Zenith Tropospheric Delay (1994-2006) and climate implications. Journal of Geophysical Research 112, D09110.

Keckhut, P., Wild, J.D., Gelman, M., Miller, A.J., Hauchecorne, A., 2001. Investigations on long-term temperature changes in the upper stratosphere using lidar data and NCEP analyses. Journal of Geophysical Research 106 (D8), 7937–7944.

King, R.W., Bock, Y., 1999. Documentation for the GAMIT GPS Analysis Software. Massachusetts Institute of Technology, Cambridge Mass.

Krügel, M., Thaller, D., Tesmer, V., Rothacher, M., Angermann, D., Schmid, R., 2007. Tropospheric parameters: combination studies based on homogeneous VLBI and GPS data. Journal of Geodesy 81, 515–527.

Niell, A.E., 1996. Global mapping functions for the atmosphere delay at radio wavelength. Journal of Geophysical Research 101 (B2), 3227–3246.

Niell, A.E., Coster, A.J., Solheim, F.S., Mendes, V.B., Toor, P.C., Langley, R.B., Upham, C.A., 2001. Comparison of measurements of atmospheric wet delay by radiosonde, water vapor radiometer, GPS, and VLBI. Journal of Atmospheric and Oceanic Technology 18, 830–850.

Petrov, L., Boy, J-P., 2004. Study of the atmospheric pressure loading signal in very long baseline interferometry observations. Journal of Geophysical Research 109, B03405.

Schuh, H., Boehm, J., 2003. Determination of tropospheric parameters within the IVS Pilot Project. Österreichische Zeitung für Vermessung & Geoinformation (VGI) 1/2003, 14–20.

Snajdrova, K., Boehm, J., Willis, P., Haas, R., Schuh, H., 2005. Multi-technique comparison of tropospheric zenith delays derived during the CONT02 campaign. Journal of Geodesy 79 (10-11).

Swinbank, R., Orris, R.L., Wu, D.L., 1999. Stratospheric tides and data assimilation. Journal of Geophysical Research 104, 16929–16947.

Titov, O., Tesmer, V., Boehm, J., 2004. OCCAM v.6.0 Software for VLBI Data Analysis. In: Vandenberg, N.R., Baver, K.D., (eds), IVS 2004 General Meeting Proceedings. Ottawa, 9–11 February, pp 267–271

Vial, F., 1989. Tides in the middle atmosphere. Journal of Atmospheric and Terrestrial Physics 51 (1), 3–17.

Whiteman, C.D., Bian, X., 1996. Solar semidiurnal tides in the troposphere: detection by radar profiles. Bulletin of the American Meteorological Society 77, 529–542.